Single-photon detectors combining high efficiency, high detection rates, and ultra-high timing resolution

Iman Esmaeil Zadeh, Johannes W. N. Los, Ronan B. M. Gourgues, Violette Steinmetz, Gabriele Bulgarini, Sergiy M. Dobrovolskiy, Val Zwiller, and Sander N. Dorenbos

Citation: APL Photonics **2**, 111301 (2017);
View online: https://doi.org/10.1063/1.5000001
View Table of Contents: http://aip.scitation.org/toc/app/2/11
Published by the American Institute of Physics

Single-photon detectors combining high efficiency, high detection rates, and ultra-high timing resolution

Iman Esmaeil Zadeh,[a] Johannes W. N. Los, Ronan B. M. Gourgues, Violette Steinmetz, Gabriele Bulgarini, Sergiy M. Dobrovolskiy, Val Zwiller,[b] and Sander N. Dorenbos
Single Quantum B.V., 2628 CH Delft, The Netherlands

(Received 12 August 2017; accepted 17 October 2017; published online 7 November 2017)

Single-photon detection with high efficiency, high time resolution, low dark counts, and high photon detection rates is crucial for a wide range of optical measurements. Although efficient detectors have been reported before, combining all performance parameters in a single device remains a challenge. Here, we show a broadband NbTiN superconducting nanowire detector with an efficiency exceeding 92%, over 150 MHz photon detection rate, and a dark count rate below 130 Hz operated in a Gifford-McMahon cryostat. Furthermore, with careful optimization of the detector design and readout electronics, we reach an ultra-low system timing jitter of 14.80 ps (13.95 ps decoupled) while maintaining high detection efficiencies (>75%). https://doi.org/10.1063/1.5000001

Single-photon detectors play a pivotal role in quantum optics. They have demonstrated advantages in quantum cryptography,[1] experiments with quantum dots and color centers,[2,3] spin-photon entanglement,[4] laser ranging,[5] biological imaging,[6] and CMOS testing,[7] among others. Several technologies have been developed for the purpose of single-photon detection, with the two most promising ones being semiconducting avalanche photodiodes (APDs) and superconducting nanowire single-photon detectors (SNSPDs). Most APDs can operate in room temperature and are relatively inexpensive. However, despite their significant developments over the past decade, the combination of their detection efficiency (particularly in the infrared range), dark count rate, and timing jitter still does not meet the stringent requirements of modern quantum optics experiments.[8] On the other hand, SNSPDs because of their sensitivity in the near-infrared, low dark count rate, and good timing properties have been the detector of choice in many demanding applications, allowing in principle to combine high performance in all key parameters: very high efficiencies, high timing resolution, low dark counts, and high detection rates.

Efficient SNSPDs, achieving 93% system detection efficiency, based on a-WSi have been demonstrated.[9] Additionally, for the case of waveguide coupled detectors, an on-chip efficiency >90%, <20 ps timing jitter, and millihertz dark count rates have been reported.[10,11] However, when the source is not integrated on the same chip as the detector, for achieving high system detection efficiency, the devices must be directly fiber coupled. The need for fiber coupling of the detectors imposes stringent requirements on the geometry of the device and exposes the detector to the blackbody radiation which is coupled to the guided modes of the fiber, increasing the dark count rates in the devices. In a recent work,[12] a NbN detector having a high efficiency in conjunction with the low jitter and low dark count rate has been shown. Unfortunately, no high count rate performance for this detector is reported. Furthermore, this detector requires the use of lensed fibers which makes the optical alignment of the device more complicated.

[a]Electronic mail: iman@singlequantum.com
[b]Also at Department of Applied Physics, Royal Institute of Technology (KTH), SE-106 91 Stockholm, Sweden.

In all the aforementioned cases, the detectors, for their best performance, must operate at lower temperatures (<1 K for a-WSi detector and <2 K for best reported NbN detector) than the base temperature of typical Gifford-McMahon closed cycle systems (2.4–3 K). This limits the choice of a cryostat and increases the complexity. Here we report, a self-aligned fiber coupled SNSPD with a high efficiency, low dark count rate, low timing jitter, and high count rate. Unlike prior demonstration of >90% efficiency SNSPDs, our detectors are mounted in a conventional Gifford-McMahon cryostat with the base temperature of ~2.5 K allowing for a cost-efficient implementation and months of non-stop operation.

Our detectors are fabricated on NbTiN films that are deposited using DC magnetron sputtering. Similar to Ref. 13, a 1.5-2 nm thick layer of NbO and TiO_2 is formed on top of our superconducting layer, preventing it from further oxidization. The film thickness and detector geometry define the optical absorption and its timing response and also affect the degree of saturation of internal efficiency (the probability that the absorption of a photon creates a detection pulse) in the detectors. The saturation and critical current play a crucial role in the optimization of the jitter, efficiency, and count rate performance of the devices; this relationship will be discussed in more detail.

Using 3D finite-difference time-domain (FDTD) simulations, we calculated the optical absorption of a NbTiN detector on a cavity optimized for the wavelength of 1550 nm, as shown in Fig. 1(a). The results indicate that film thicknesses between 10 and 12 nm will provide maximum optical absorption in the detector. However, for those thicknesses, it is hard to achieve saturation of the internal detection. To guarantee high absorption while achieving a reasonable saturation of the internal efficiency and good timing response, as will be discussed further in this paper (Figs. 3 and 4), we chose a film thickness of 8.4 nm.

After sputtering the NbTiN film, metal contacts are formed using optical lithography and Cr/Au evaporation. Then nanowires are fabricated on gold mirrors separated by a layer of SiO_2 serving as a cavity. The cavity is designed to maximize the detector absorption at the desired wavelength range of

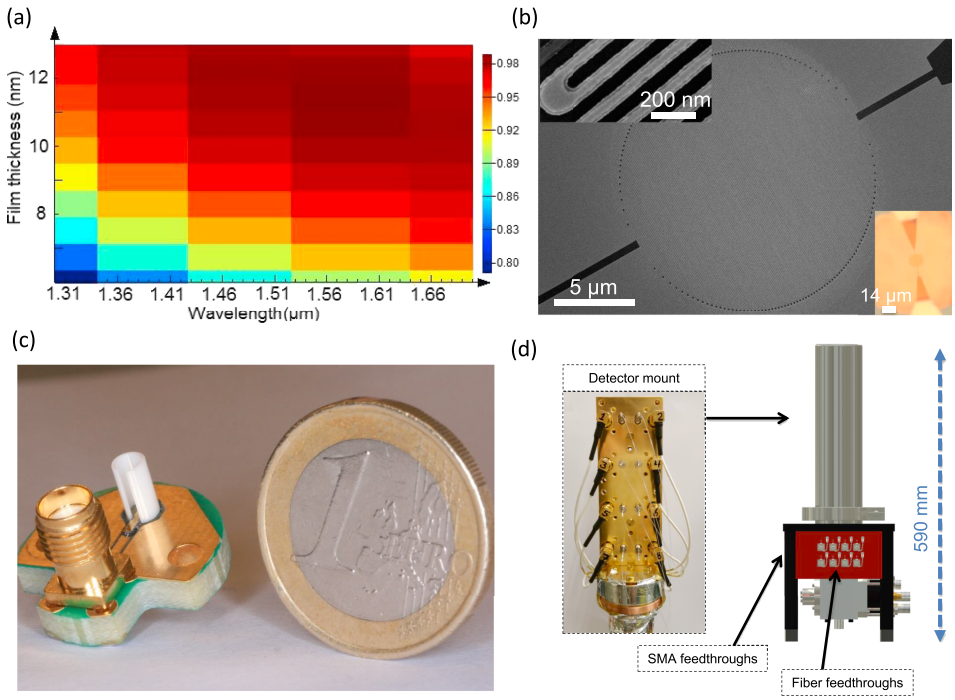

FIG. 1. (a) A 3D FDTD simulation of optical absorption of SNSPD versus wavelength and film thickness. (b) A scanning electron microscope image of a fabricated detector. The top inset is a zoomed picture of the device. The bottom inset is an optical microscope photo demonstrating a detector on a gold mirror. (c) Complete device after mounting in a FC mating sleeve, gluing to the printed circuit board, and wire bonding to the transmission lines. (d) Left: the cold finger with mounted detectors and right: a rendered picture of the cryostat.

1310-1625 nm.[14] We optimized the nanowire width to be 50 nm, the filling factor to be 0.42, and the diameter of the detector to be 14 μm. The nanowires were patterned using hydrogen silsesquioxane e-beam resists and were transferred to the NbTiN layer by dry etching in SF_6 and O_2 chemistry. Figure 1(b) presents an SEM image of a fabricated device. The inset in Fig. 1(b) shows a magnified view of the detector, and the bottom inset provides an optical microscope picture, showing the device fabricated on a gold mirror. For fiber coupling of the detectors, using a Bosch process similar to Refs. 15 and 16, the devices were formed in a keyhole shape and then fixed in FC-mating sleeves. For electrical bias and readout, the detectors were glued and bonded to printed circuit boards (PCBs), as shown in Fig. 1(c). Finally, the devices were mounted in a compact Gifford-McMahon cryostat with antireflection coated fibers and coaxial feedthroughs as shown in Fig. 1(d).

To evaluate the efficiency of the detectors, a fiber-coupled laser was attenuated to a level corresponding to 100-150 kphotons/s and then connected to the detectors using a standard FC-FC connector. We used NIST traceable attenuators and powermeters, and the laser power was stable within 1%-1.5% during the measurements. The measurement setup is shown in Fig. 2(a). We estimate the total measurement error to be better than ±4%. More details on the setup and the contribution of each piece of equipment to the measurement error are provided in the supplementary material.

For telecom detectors, to reach the lowest dark count rates at high efficiencies, we spool the fiber around a mandrel[17] with a diameter of 23 mm. The spooling of the fiber filters the longer wavelength blackbody radiation, coupled into the fiber modes, and hence, the dark counts are reduced. However, it also limits the bandwidth of the detector.

The result of the efficiency measurement at 1310 nm is shown in Fig. 2(b). Each point in Fig. 2(b) is an average over four measurements each integrated for 100 ms. The efficiency curve saturates at values between 91.5% and 93.3%. The dark count rate at >90% efficiency level is below 150 Hz. It must be noted that to measure the true system detection efficiency, avoiding

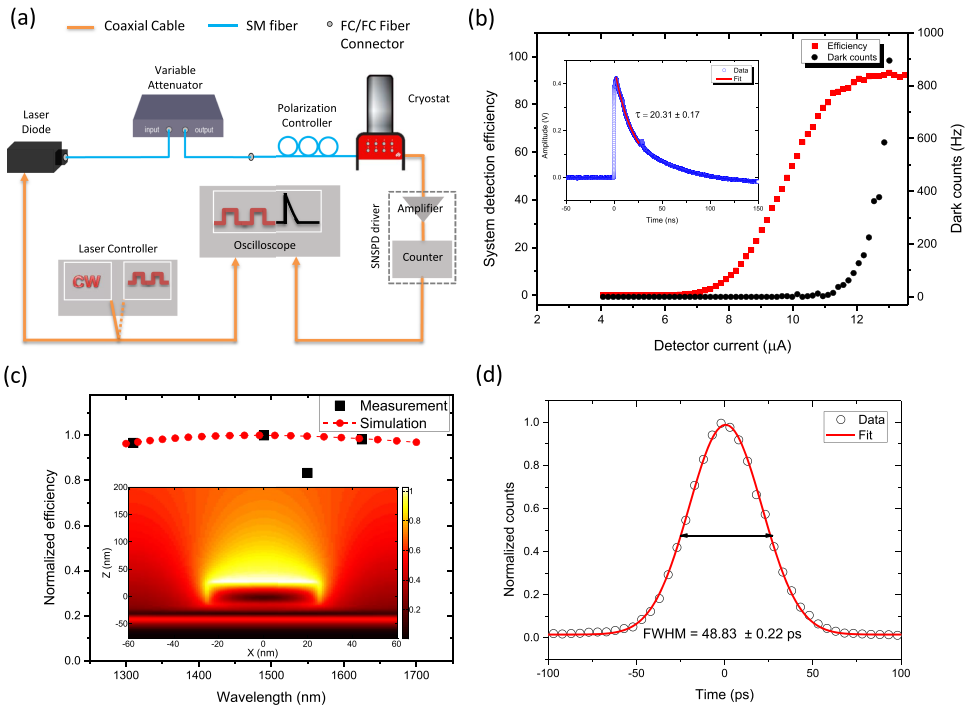

FIG. 2. (a) Schematic of the setup used to characterize the detectors. The performance of our detectors is evaluated for both continuous and pulsed excitations. (b) The system detection efficiency (for O-band photons) and dark count versus current. The inset presents a captured detection pulse from our SNSPD; the fitted data are an exponential with a decay constant of 20.31 ns. (c) Measured versus simulated normalized detection efficiency for wavelengths of 1310 nm, 1490 nm, 1550 nm, and 1625 nm. The inset is a cut of the intensity profile of light for the simulated structure. (d) Timing jitter measurement of the SNSPD.

over-estimations, we subtract the dark counts and consider the fact that the power measurement was done on an uncoated fiber while the detector is connected to an antireflection coated fiber. The mentioned contribution accounts for ~3.6% which has been deducted from each measurement point (the not-corrected measured peak efficiency is ~97%). The inset in Fig. 2(b) shows a detection pulse from the SNSPD with a recovery time constant of 20.31 ± 0.17 ns.

Before spooling fibers, we characterized the bandwidth of our detector as shown in Fig. 2(c). The measured efficiencies, indicated by black squares, are similar for wavelengths of 1310 nm, 1490 nm, and 1625 nm which are in close agreement with our 3D FDTD simulations, shown by red filled circles. However, the normalized efficiency at 1550 nm is lower. The latter was ruled out not to be an artifact of the measurement by repeating the experiment and checking the setup by measuring other detectors (with a different wavelength dependence behavior). One explanation, not excluding other possibilities, is an air-gap between the end-facet of the fiber and the chip[14] (also see the supplementary material). The separation between the fiber and the chip could have been caused by small particles (dust) on the detector chip.

For applications in optical communication[18,19] and quantum information processing,[20] efficient detectors at high detection rates are required. It has been shown that the recovery time of the detectors is mainly caused by the kinetic inductance of the nanowire.[21] It has also been shown that the maximum count rate is not only set by the recovery time of the detector[22] but also set by the readout circuitry. The reason for this is that the readout components can store energy that is released at a time scale much longer than the dead time. At high count rates, this persistent bias current leads to higher effective bias and extra Joule heating. To this end, a DC coupled circuit[22] and a resistive network[23] have been proposed. In this work, a resistive network has been combined with the high efficiency detector to improve the quantum efficiency at higher detection rates. This is done by letting the extra charge, stored in the readout capacitor, to dissipate through a resistor at the price of reduced amplitude of the output signal. To enhance the signal to noise ratio, the pulses from the detector were first amplified by a liquid nitrogen cooled amplifier followed by a second stage room temperature amplifier (more information about amplifiers can be found in the supplementary material). Figure 2(d) presents the results of the timing jitter measurement, the fitted data yield a jitter of FWHM = 48.83 ± 0.22 ps.

We conduct measurements on the detection rate dependence of the efficiency, both for the cases of a continuous field (see the supplementary material) and a pulsed laser. Figure 3(a) shows examples of optical pulses, captured with a fast photodiode, and their corresponding SNSPD detection events. Clearly, even at high detection rates, for every optical pulse, there is only one detection event. For each detection rate, taking a similar approach as in Ref. 24, we evaluate the efficiency of our detectors using the following equation:

$$\eta = \frac{-\ln\left(1 - \frac{SNSPD_{counts}}{f_{rep}}\right)}{\mu} \times 100\,\%, \tag{1}$$

where $SNSPD_{counts}$ is the measured count rate on the detector, f_{rep} is the repetition rate of the laser, and μ is the average number of photons in each pulse given by

$$\mu = \frac{P_{opt}\,\lambda}{hcf_{rep}}, \tag{2}$$

where P_{opt} is the input optical power, λ is the wavelength, h is the Planck constant, and c is the speed of light. Figure 3(b) presents the efficiency versus the detector count rate measured for three different wavelengths. At high excitation rates, some photons arrive before the detector bias current has fully recovered, resulting in reduced detection probability. This reduction in efficiency depends on the bias current and dead time of the detector and also on the excitation wavelength as shown in Fig. 3(c). For the case of 50 MHz pulsed excitation, photons are well separated and the efficiency is relatively insensitive to the count rate of the detector.

In Fig. 3(b), a small dip for the cases of excitation at 878 nm and 1310 nm (pulsed at 50 MHz) can be observed. We ascribe this dip to the transition from detecting photons in every second or third pulse, which induces strong baseline fluctuations, for detecting each and every consecutive pulse. This effect can be understood by comparing the insets of Fig. 3(c). At low

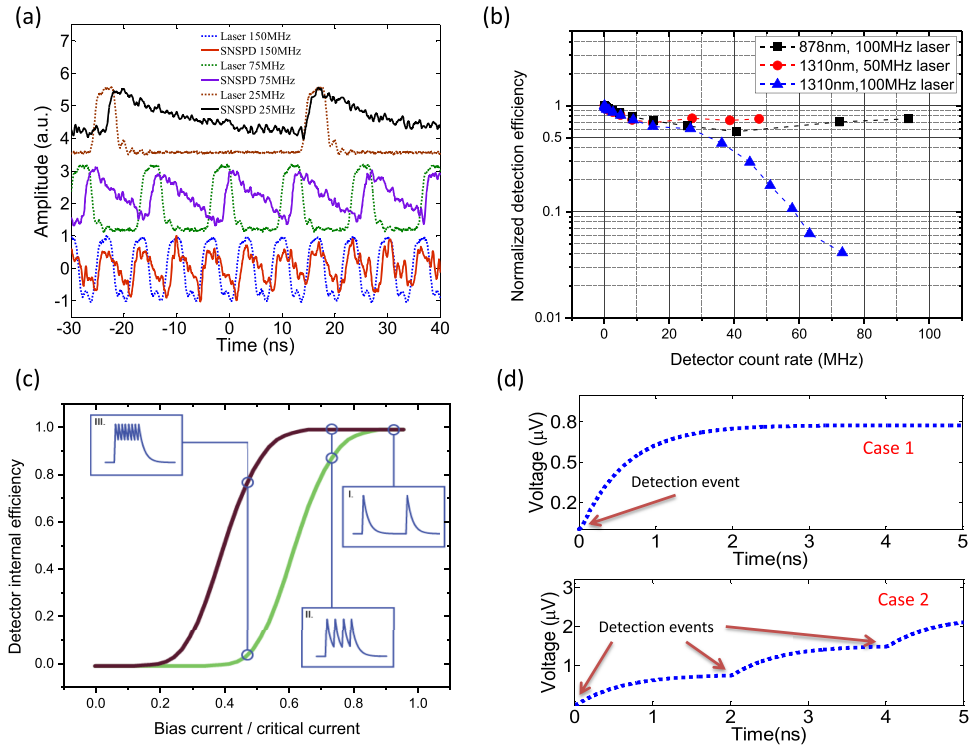

FIG. 3. (a) Oscilloscope traces of 25, 75, and 150 MHz excitation pulses and their corresponding SNSPD detection events. For each pulse, there is only one detection event. (b) Efficiency versus detection rate under pulsed excitations. (c) An illustration of the dependence of the detector internal efficiency on the separation between optical pulses. A detector with strong saturation (darker curve) can achieve higher count rates without a significant drop in efficiency. (d) Simulation of the readout capacitor voltage. If multiple detection events take place within a short time, the capacitor charges up to higher values. When the values of these charges are random, to avoid the SNSPD from latching, the detector has to be underbiased.

detection rates (region 1), the pulses are well separated and so the detector is biased normally. As the count rate approaches the repetition rates of the laser (region 3), almost all optical pulses are detected so it gives a "constant" DC shift to the detector current. This DC shift can be partially compensated by readjusting the bias current so that the effective device bias remains similar. However, when the detection rate is, for example, half of the laser repetition rate, this DC shift depends on the temporal distance between detection pulses and hence becomes random and cannot be compensated. To avoid the detector switching to the normal state with no recovery (latching), the detector bias current has to be lowered. This underbiasing reduces the internal efficiency of the detector.

At medium detection rates (comparing to the repetition rate of the laser), the stored charge on the readout capacitor can also play a role in reducing the efficiency. To better explain this effect, we simulated the readout capacitor voltage using an electrothermal model similar to Ref. 25. Figure 3(d) provides the simulation results for two examples. Case 1: only one optical pulse is detected. The capacitor charges up to a constant value. Case 2: three consecutive optical pulses are detected. The capacitor charges to a higher value in this case. For both the cases the capacitor, partially (thanks to our resistive network), discharges into the detector over a much longer time scale defined by the characteristic time constant of its discharge circuit. Similarly, only when this charging and discharging are regular, i.e., at very low or detection rates very close to the laser repetition rate, the SNSPD can be biased efficiently. It should be noted that the detector used in this simulation is a hypothetical one with fast recovery time (~1 *ns*, purely for the sake of reducing simulation time) and also may have slightly different thermal parameters (we used the values in Ref. 25) in comparison with our real devices. As we only use this simulation to explain the qualitative behavior of the readout capacitor, the exact model of the system is not of a major concern.

For many applications such as laser ranging and quantum computing with non-idealistic photons, improving the timing resolution of single-photon detectors is of prime importance. To achieve the best timing resolution, we optimized our custom readout electronics (see the supplementary material) and fixed it to a 30 K stage inside the cryostat. Furthermore, we optimized the critical current of our detectors and the rise time of its pulses. The detector's critical current and its optical absorption increase by increasing the film thickness; however, this leads to a decrease in the saturation of internal efficiency. Figure 4(a) shows histograms of critical currents for different film thicknesses. For the case of an 8.4 nm film, fabrication of narrower nanowires was required to reach a reasonable saturation. While we used 50 nm wide nanowires and higher filling factors for the highest efficiency, we could reach higher critical currents and faster pulse rise time by increasing the nanowire width to 70 nm and slightly reducing the filling factor (to about 0.4). After aforementioned improvements, we achieved a record low timing jitter of FWHM = 14.80 ± 0.05 ps as shown in Fig. 4(b). It should be added that the reported timing jitter includes the measurement instruments' contribution (intrinsic jitter is < 14 ps, see the supplementary material). Best reported SNSPDs' timing jitter achieved high time resolution at the cost of making small and low efficiency detectors.[26,27] In this work, we present a standard size fiber-coupled detector which combines an ultra-low timing jitter and a high efficiency in the O-band (>75%, see the supplementary material). By optimizing the following parameters: first, reducing the filling factor, improving the rise time of the detection pulses; second, slight reduction of the nanowire width, to improve the internal efficiency of the detector (while still maintaining a high critical current); and third, adding top dielectric layers, enhancing optical absorption; both jitter and the detection efficiency can be improved.

In conclusion, we have demonstrated a single-photon detector combining very high efficiency, low dark count rate, low timing jitter, and high detection rates. Moreover, our detectors operate in a Gifford-McMahon cryostat. Optimized devices provided unprecedented timing resolution. The technology presented in this paper opens the way for the realization of efficient and high throughput optical communication, demanding quantum optical experiments.

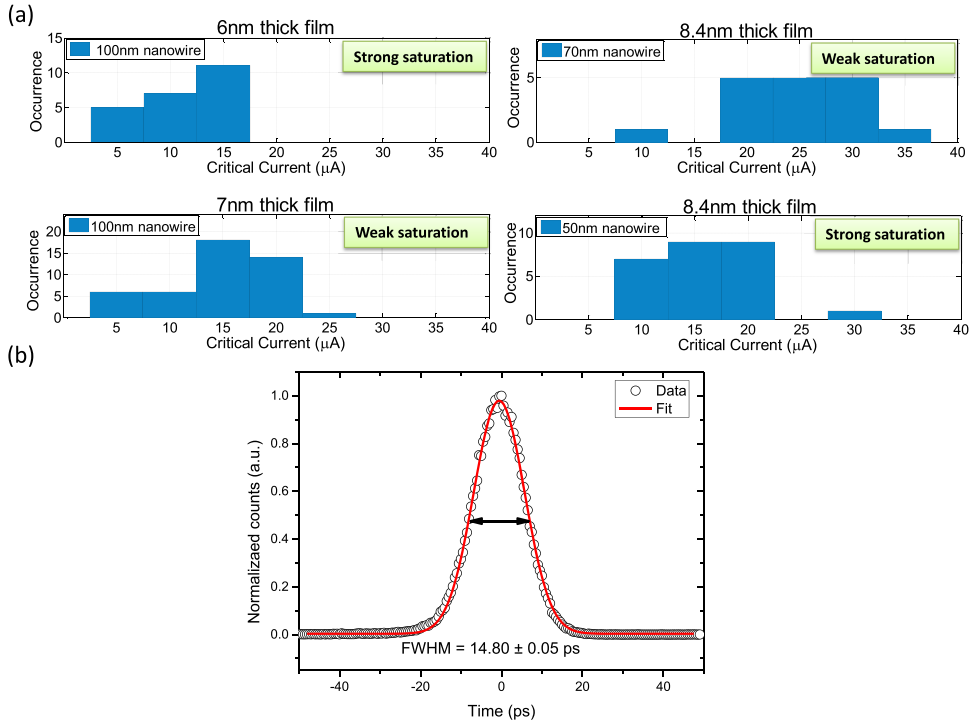

FIG. 4. (a) Histograms of critical currents for different film thicknesses. For the case of an 8.4 nm film, fabrication of narrower nanowires was required to achieve saturation of internal efficiency. (b) An optimized SNSPD with a timing jitter of FWHM = 14.80 ± 0.05 ps. This detector also reaches high efficiency in O-band (see the supplementary material).

See supplementary material for more details on the measurement setup and measurement error and extra information on high count rate and jitter measurements.

Ronan B. M. Gourgues acknowledges support by the European Commission via the Marie-Sklodowska Curie action Phonsi (H2020-MSCA-ITN-642656).

[1] N. Gisin, G. Ribordy, W. Tittel, and H. Zbinden, Rev. Mod. Phys. **74**, 145 (2002).
[2] M. Felle, J. Huwer, R. M. Stevenson, J. Skiba-Szymanska, M. B. Ward, I. Farrer, R. V. Penty, D. A. Ritchie, and A. J. Shields, Appl. Phys. Lett. **107**, 131106 (2015).
[3] D. J. Christle, A. L. Falk, P. Andrich, P. V. Klimov, J. U. Hassan, N. T. Son, E. Janzén, T. Ohshima, and D. D. Awschalom, Nat. Mater. **14**, 160 (2015).
[4] K. D. Greve, L. Yu, P. L. McMahon, J. S. Pelc, C. M. Natarajan, N. Y. Kim, E. Abe, S. Maier, C. Schneider, M. Kamp, S. Höfling, R. H. Hadfield, A. Forchel, M. M. Fejer, and Y. Yamamoto, Nature **491**, 421 (2012).
[5] A. McCarthy, N. J. Krichel, N. R. Gemmell, X. Ren, M. G. Tanner, S. N. Dorenbos, V. Zwiller, R. H. Hadfield, and G. S. Buller, Opt. Express **21**, 8904 (2013).
[6] A. Pe'er, Y. Bromberg, B. Dayan, Y. Silberberg, and A. A. Friesem, Opt. Express **15**, 8760 (2007).
[7] J. Zhang, N. Boiadjieva, G. Chulkova, H. Deslandes, G. N. Gol'tsman, A. Korneev, P. Kouminov, M. Leibowitz, W. Lo, R. Malinsky, O. Okunev, A. Pearlman, W. Slysz, K. Smirnov, C. Tsao, A. Verevkin, B. Voronov, K. Wilsher, and R. Sobolewski, Electron. Lett. **39**, 1086 (2003).
[8] J. Zhang, M. A. Itzler, H. Zbinden, and J.-W. Pan, Light Sci. Appl. **4**, e286 (2015).
[9] F. Marsili, V. B. Verma, J. A. Stern, S. Harrington, A. E. Lita, T. Gerrits, I. Vayshenker, B. Baek, M. D. Shaw, R. P. Mirin, and S. W. Nam, Nat. Photonics **7**, 210 (2013).
[10] W. Pernice, C. Schuck, O. Minaeva, M. Li, G. Goltsman, A. Sergienko, and H. Tang, Nat. Commun. **3**, 1325 (2012).
[11] C. Schuck, W. H. P. Pernice, and H. X. Tang, Sci. Rep. **3**, 210 (2013).
[12] W. J. Zhang, L. X. You, H. Li, J. Huang, C. L. Lv, L. Zhang, X. Y. Liu, J. J. Wu, Z. Wang, and X. M. Xie, Sci. China Phys. Mech. **60**(12), 120314 (2017).
[13] R. Cheng, X. Guo, X. Ma, L. Fan, K. Y. Fong, M. Poot, and H. X. Tang, Opt. Express **24**, 27070 (2016).
[14] M. G. Tanner, C. M. Natarajan, V. K. Pottapenjara, J. A. O'Connor, R. J. Warburton, R. H. Hadfield, B. Baek, S. Nam, S. N. Dorenbos, E. B. Ureña, T. Zijlstra, T. M. Klapwijk, and V. Zwiller, Appl. Phys. Lett. **96**, 221109 (2010).
[15] S. N. Dorenbos, R. W. Heeres, E. F. C. Driessen, and V. Zwiller, e-print arXiv:1109.5809 [physics.optics] (2011).
[16] A. J. Miller, A. E. Lita, B. Calkins, I. Vayshenker, S. M. Gruber, and S. W. Nam, Opt. Express **19**, 9102 (2011).
[17] K. Smirnov, Y. Vachtomin, A. Divochiy, A. Antipov, and G. Goltsman, Appl. Phys. Express **8**, 022501 (2015).
[18] J. Yin, Y. Cao, S.-B. Liu, G.-S. Pan, J.-H. Wang, T. Yang, Z.-P. Zhang, F.-M. Yang, Y.-A. Chen, C.-Z. Peng, and J.-W. Pan, Opt. Express **21**, 20032 (2013).
[19] G. Vallone, D. Dequal, M. Tomasin, F. Vedovato, M. Schiavon, V. Luceri, G. Bianco, and P. Villoresi, Phys. Rev. Lett. **116**, 253601 (2016).
[20] R. H. Hadfield, Nat. Photonics **3**, 696 (2009).
[21] A. J. Kerman, E. A. Dauler, W. E. Keicher, J. K. W. Yang, K. K. Berggren, G. Gol'tsman, and B. Voronov, Appl. Phys. Lett. **88**, 111116 (2006).
[22] A. J. Kerman, D. Rosenberg, R. J. Molnar, and E. A. Dauler, J. Appl. Phys. **113**, 144511 (2013).
[23] Q. Zhao, T. Jia, M. Gu, C. Wan, L. Zhang, W. Xu, L. Kang, J. Chen, and P. Wu, Opt. Lett. **39**, 1869 (2014).
[24] A. E. Lita, A. J. Miller, and S. W. Nam, Opt. Express **16**, 3032 (2008).
[25] J. K. W. Yang, A. J. Kerman, E. A. Dauler, V. Anant, K. M. Rosfjord, and K. K. Berggren, IEEE Trans. Appl. Supercond. **17**, 581 (2007).
[26] V. Shcheslavskiy, P. Morozov, A. Divochiy, Y. Vakhtomin, K. Smirnov, and W. Becker, Rev. Sci. Instrum. **87**, 053117 (2016).
[27] J. Wu, L. You, S. Chen, H. Li, Y. He, C. Lv, Z. Wang, and X. Xie, Appl. Opt. **56**, 2195 (2017).